

Technical considerations in longitudinal multispectral small animal molecular imaging

Matthew B. Bouchard

Northeastern University
Department of Physics
360 Huntington Avenue
Boston, Massachusetts 02115

Sarah A. MacLaurin

Novartis Institutes for BioMedical Research, Inc.
Discovery Technologies
250 Massachusetts Avenue
Cambridge, Massachusetts 02139

Peter J. Dwyer James Mansfield Richard Levenson

Cambridge Research & Instrumentation, Inc. (CRI)
35-B Cabot Road
Woburn, Massachusetts 01801

Thomas Krucker

Novartis Institutes for BioMedical Research, Inc.
Discovery Technologies
250 Massachusetts Avenue
Cambridge, Massachusetts 02139

Abstract. In a previous study, we investigated physical methods to reduce whole-body, diet-related autofluorescence interference in several mouse strains through changes in animal diet. Measurements of mice with an *in vivo* multispectral imaging system over a 21-day period allowed for the quantification of concentration changes in multiple *in vivo* fluorophores. To be an effective instrument, a multispectral imaging system requires *a priori* spectral knowledge, the form and importance of which is not necessarily intuitive, particularly when noninvasive *in vivo* longitudinal imaging studies are performed. Using an optimized spectral library from a previous autofluorescence-reduction study as a model, we investigated two additional spectral definition techniques to illustrate the results of poor spectral definition in a longitudinal fluorescence imaging study. Here we systematically evaluate these results and show how poor spectral definition can lead to physiologically irrelevant results. This study concludes that the proper selection of robust spectra corresponding to each specific fluorescent molecular label of interest is of integral importance to enable effective use of multispectral imaging techniques in longitudinal fluorescence studies. © 2007 Society of Photo-Optical Instrumentation Engineers. [DOI: 10.1117/1.2799188]

Keywords: multi-spectral imaging; autofluorescence reduction; spectral definition.

Paper 07017SSR received Jan. 15, 2007; revised manuscript received Apr. 11, 2007; accepted for publication May 16, 2007; published online Oct. 24, 2007.

1 Introduction

As more potential drugs make it through the drug discovery pipeline to the clinic, the challenge of successfully navigating new compounds from bench to bedside becomes more difficult, regularly requiring many years and enormous expenditures.¹⁻³ New technological advances that shorten the time required for and cut the costs of drug discovery are being rapidly integrated into the drug discovery process. The molecular biology revolution of the early 1990s brought the concept of target-specific therapy; following the identification of specific chemical mechanisms that control the progression of a disease, drug compounds can be developed to directly modulate pathways.^{3,4}

One of the more recent technological advances with great potential to influence drug discovery is fluorescence molecular imaging, the use of modern fluorescence imaging techniques to noninvasively monitor molecular events *in vivo*.⁵ Combined with the insights of molecular biology, molecular imaging has had its greatest impact thus far in the preclinical testing and verification phases of the drug discovery pipeline.⁶ In addition to providing the capability to perform longitudinal studies on the same animal, allowing each animal to act as its own control, fluorescence molecular imaging techniques can simultaneously exploit a wide range of currently available

fluorophores to study multiple disease readouts throughout a longitudinal study with minimal or no modification of a given disease model's innate physiology.⁷ *In vivo* longitudinal studies probing drug specificity, efficacy, toxicity, and disease progression over several weeks can be performed using multiplexed fluorophores.⁸

Multiplexing provides additional readouts that would be difficult to acquire using other common optical imaging-based experimental techniques. For instance, both bioluminescence imaging^{9,10} and optical coherence tomography (OCT)¹¹ are typically limited to a single mode of contrast. In addition, studies employing traditional histological techniques using highly specific fluorophores tend to be time-consuming, require large groups of animals, and are normally limited in the number of study readouts that can be obtained from a single sample. The strong push for multiplexed assays *in vivo* is based on the emergence of destructive technologies that provide multiple readouts from a limited amount of material. Gene and protein array technologies (genomics and proteomics) have enabled researchers to realize a wealth of new information related to patterns of gene alterations and expression. Unfortunately, these data are typically generated from homogenized tissue samples and do not maintain any reference to the morphology or spatial context of gene expression. Similarly, for isolated cells, flow cytometry has been extremely useful for looking at the expression of multiple markers. Multispectral imaging methods, in both microscopic and

Address all correspondence to: Dr. Thomas Krucker, Novartis Institutes for BioMedical Research, Inc., Discovery Technologies, 250 Massachusetts Avenue, Cambridge, MA 02139. Tel: 617-871-3763; Fax: 617-871-4105; E-mail address: thomas.krucker@novartis.com.

in vivo imaging can allow the simultaneous visualization and quantization of multiple markers while also retaining the spatial relationships among them.¹²

Even with these experimental strengths, fluorescence molecular imaging has not yet proven itself to be the panacea many researchers would like it to be. Highly specific targeted probes exist, but *in vivo* they are often masked by autofluorescence or emit such low levels of light that make adequate detection of their fluorescent signal tenuous at best.¹³ *In vivo* autofluorescence is commonly defined as unwanted fluorescence emission from unlabeled sources, such as collagen, elastin, and beta carotene, and/or oils, pigments, and proteins from ingested food. *In vivo* autofluorescence is a whole-body effect that cannot be completely removed through physical means. Earlier studies have indicated that the food-related component of *in vivo* autofluorescence could potentially be reduced through changes in diet.¹⁴ Even without interference from tissue autofluorescence, the multiplexing of exogenous fluorophores offers a great deal of experimental flexibility, but it is frequently difficult, if not impossible, to separate multiple emission spectra using traditional, barrier-type optical filters due to the close spectral overlap of many common fluorophores.¹² Three-dimensional (3D) tomographic fluorescence molecular imaging techniques can provide a wealth of spatial information but often require large amounts of time for data acquisition and analysis, suffer from the interference of autofluorescence, and impose unwelcome experimental constraints in longitudinal drug studies that routinely employ relatively large groups of animals ($n > 20$) over multiweek periods. Also, some 3D tomographic imaging techniques place considerable strain on a disease model's physiology during data acquisition (i.e., length of time under anesthesia), potentially altering the results of a drug study. Two-dimensional (2D) planar fluorescence imaging techniques that place little to no strain on a disease model's physiology during data acquisition have become preferred in many drug discovery laboratories due to their relatively high-throughput data acquisition and simple, rapid data analyses.⁹ Experimental and commercially available planar multispectral imaging systems have been developed to address the common problems encountered in *in vivo* fluorescence molecular imaging.^{13,15–18} Mathematical separation of autofluorescence from the fluorophore(s) of interest via spectral unmixing increases the sensitivity of the measurement in a manner not possible physically and greatly improves the quantitative aspects of the data by providing single and composite quantitative images of the spatial distribution of fluorophore concentrations *in vivo*. The mathematical techniques for spectral unmixing are similar to those well known in the nonimaging spectroscopy community and typically rely on least-squares fitting algorithms with constraints such as nonnegativity of components.^{19–22}

Multispectral imaging techniques require a certain amount of *a priori* spectral knowledge, the form and importance of which is not necessarily intuitive, to be effective instruments in longitudinal studies. Algorithms employed to determine “pure” spectral components require previous knowledge of at least one pure spectrum, typically autofluorescence detected at the surface of an animal in an *in vivo* study. Provided an appropriate algorithm, experiments employing exogenous fluorophores can find the required *a priori* spectral knowledge rather simply. Exogenous fluorophore spectra can be calcu-

lated from a background autofluorescence spectrum sampled from a control animal and a mixed fluorescence spectrum sampled from appropriate regions of a fluorescently labeled animal using a scaled subtraction algorithm, because multiplexed spectral intensity values combine linearly. Experiments employing poorly defined exogenous fluorophores, or lacking exogenous fluorophores all together, require robust spectral definition of the physiological components of interest to be effective.

Recently, we completed a study investigating physical methods to reduce whole-body autofluorescence in several mouse strains through changes in animal diet. The study tracked the effect on skin autofluorescence intensity caused by changing the diets of three common strains of laboratory mice from a standard fluorescent chow diet containing chlorophyll to one of four weakly fluorescent, chlorophyll-free diets. Concentration changes in skin autofluorescence and food-related (chlorophyll) fluorescence in the gut were tracked over a 21-day period using the CRi Maestro, a commercially available planar multispectral imaging system. It was found that an effective longitudinal study was not possible without robust spectral definition of skin autofluorescence. Chlorophyll fluorescence did not remain confined to the digestive system as one might initially assume. Surprisingly, fluorescence related to chlorophyll in a standard murine chow, or at least fluorescence with the same spectrum as the standard murine chow found in the gut, appeared to be present not only in the gut but also across the entire surface of the animal, complicating a robust spectral definition of skin autofluorescence.²³

We are currently unaware of any previous report that systematically investigated the physiological relevance of results obtained when varying the defined component spectra in an *in vivo* multispectral imaging study. This report investigates potential errors resulting from differing spectral definitions and illustrates how to recognize and avoid them. Here we present the experimental methods and results of three investigated spectral definition techniques. The third technique described herein is the technique most capable of producing robust results within the constraints of the autofluorescence-reduction study's design. The other two otherwise-intuitive spectral definition techniques were investigated to provide comparisons to the robust technique and examples of the results produced by poor spectral definition.

2 Materials and Methods

2.1 Autofluorescence-Reduction Study

Eight male mice from three strains, CD-1, C57BL/6, and Hsu nu/nu, were imaged before (Standard Chow—“Baseline”), during (Chlorophyll Free—“No Glow”), and after (Return to Standard Chow—“Return”) being fed Harlan Teklad's chlorophyll-free purified diet, TD97184 (Fig. 1). The standard chow was Purina's Lab Diets #5053. The baseline phase lasted 6 days, the no-glow phase lasted 14 days, and the return phase lasted 7 days. Multispectral image cubes were captured with a CRi Maestro *In Vivo* Imaging System (Woburn, Massachusetts). Ventral images were taken throughout the study with the abdomens of the C57BL/6 and CD-1 strains depilated to remove highly absorbing, fluorescing, and scattering hair with a Phillips Norelco™ electric shaver (Phillips, New York City, New York) and/or Nair™ hair removal cream

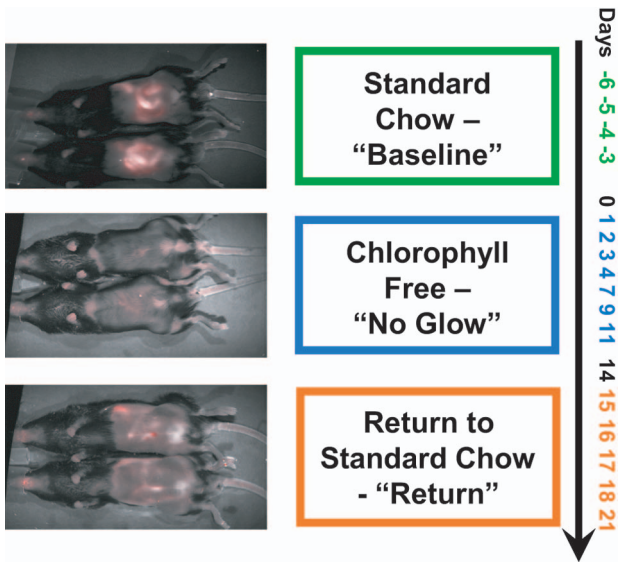


Fig. 1 Skin autofluorescence reduction study outline. Six days of baseline imaging while on a standard chow diet (Purina, Lab Diets 5053) were followed by 11 days on a no-glow chlorophyll-free purified diet (Harlan Teklad, TK97184). Seven days of return-to-standard-chow imaging completed the study. Imaging days are shown at right of the study timeline with sample raw multispectral image cubes of C57BL/6 mice shown on the left. The small subset of data from 2 days within each phase of the study presented herein is representative of the time-dependent behavior of the more densely sampled time course.

(Church and Dwight Company, Inc., Princeton, New Jersey). Changes in the concentration of chlorophyll fluorescence localized in the gut and skin autofluorescence away from the gut were tracked using the spectral unmixing algorithm and region of interest (ROI) measurements in the Maestro software. Animal handling and care was conducted in accordance with the Animal Care and Use Committee (ACUC) at the Novartis Institutes for BioMedical Research, Inc. in Cambridge, Massachusetts. All data presented herein was acquired from one strain, C57BL/6, to simplify the analysis.

2.2 Spectral Definition Techniques

Herein, the term “skin autofluorescence” is used to describe fluorescence emitted from endogenous murine fluorophores present in the skin, and “chlorophyll fluorescence” is used to describe fluorescence associated with the digested derivatives of standard alfalfa-containing rodent chow, of which chlorophyll and its derivatives are the most significant fluorescent component.^{14,24} The intensity and spectral shape of chlorophyll fluorescence is highly dependent on the chemical content of the chosen chlorophyll-containing diet. In the autofluorescence-reduction study, the intensity of chlorophyll fluorescence appeared strongest from the skin above the digestive system (gut) due to the direct fluorescence emitted by chlorophyll-related components in the digestive system while a weaker signal with an identical spectral signature was detectable across the entire surface of the animal, with local accumulations on the snout and paws, in the bladder, and on the base of the tail (see chlorophyll fluorescence component image, day 7, Fig. 6). “Mixed fluorescence” is used to de-

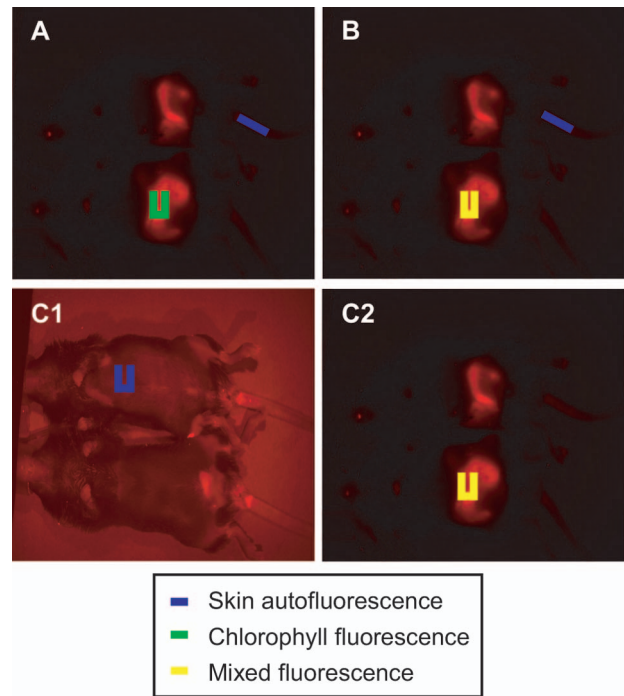


Fig. 2 Sampling locations differed spatiotemporally across the three investigated spectral definition techniques. (a) Technique 1 sampled skin autofluorescence from the tail and chlorophyll fluorescence from the gut on a baseline day. This technique did not perform a spectral calculation to determine the pure shapes of the defined spectra. (b) Technique 2 sampled skin autofluorescence from the tail and mixed fluorescence from the gut on a baseline day. The skin autofluorescence spectrum was subtracted from the mixed fluorescence spectrum, resulting in a pure chlorophyll fluorescence spectrum. (c) Technique 3 achieved robust spectral definition by measuring skin autofluorescence from the upper abdominal region on the 11th day on a chlorophyll-free diet (c1) and a mixed fluorescence spectrum from the gut on a baseline day (c2). The skin autofluorescence spectrum was subtracted from the mixed fluorescence spectrum, resulting in a pure chlorophyll fluorescence spectrum. All experimentally sampled spectra were averaged across two animals using the imaging system’s standard software.

scribe the whole-body, spectrally mixed signal of skin autofluorescence and chlorophyll fluorescence. All experimentally sampled spectra were averaged across two animals using the Maestro software.

Three spectral definition techniques were investigated, the first two of which were selected for comparison to the third’s robust spectral definition. The first comparison technique (technique 1) sampled skin autofluorescence from the tail and chlorophyll fluorescence over the gut of animals in the baseline phase, effectively characterizing chlorophyll fluorescence as mixed fluorescence [blue and green lines, respectively, Fig. 2(a); resulting spectra Fig. 3(a)]. This technique did not perform a spectral calculation to determine the pure shapes of the defined spectra. This spectral definition technique suffers from the lack of a signature, or pure spectrum, for the chlorophyll fluorescence component.

The second spectral definition technique for comparison averaged skin autofluorescence spectra sampled from the tail of animals in the baseline phase [blue line, Fig. 2(b)]. This region did not show strong chlorophyll fluorescence during

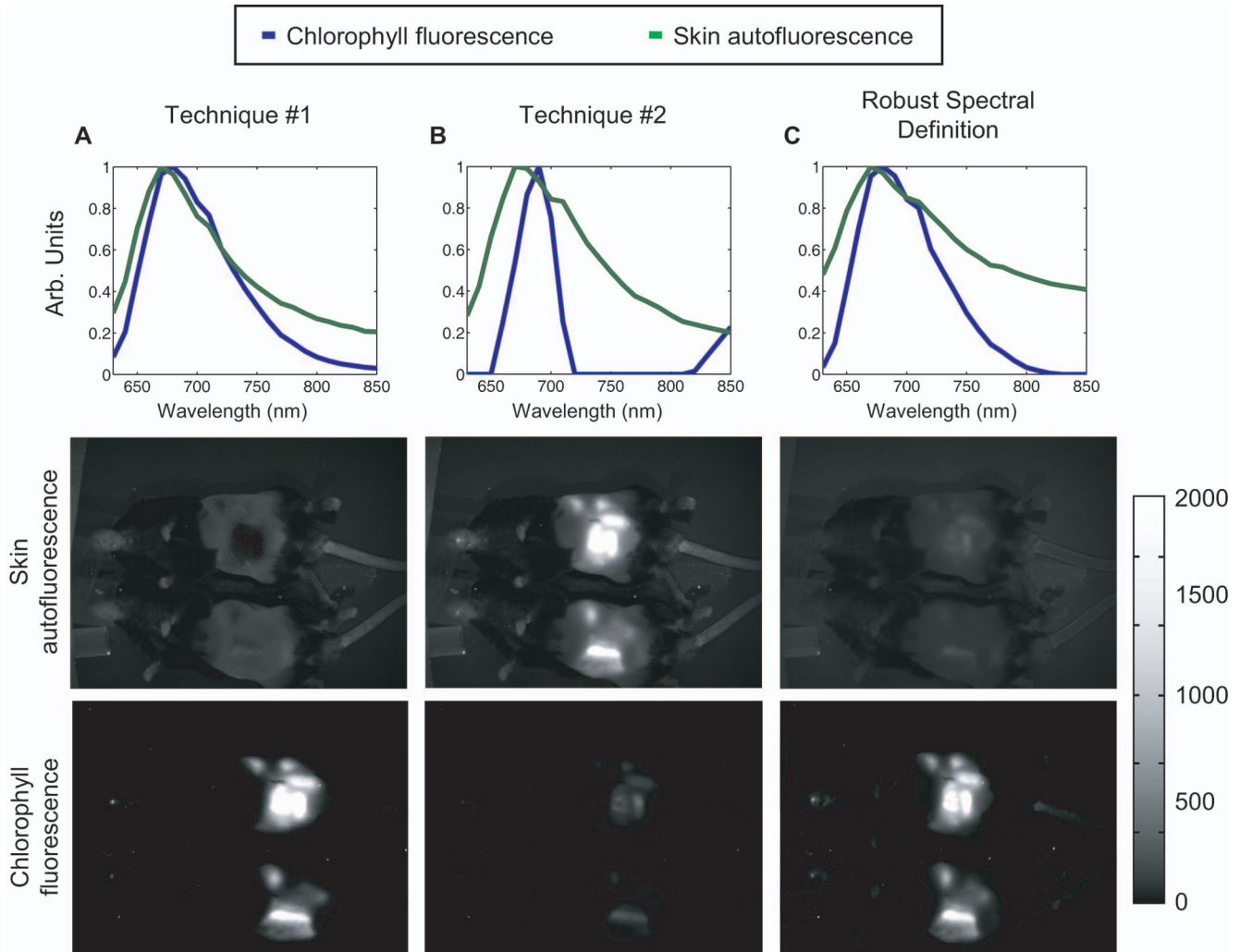


Fig. 3 Skin autofluorescence, chlorophyll fluorescence spectra, and corresponding unmixed spectral component images from a baseline day. Robust spectral definition produces the most physiologically relevant results, while the two comparison techniques are shown to produce physiologically implausible results. (a) Technique 1 results in unmixed skin autofluorescence component images exhibiting zero concentration in the gut, which is contrary to the expectation that the fluorophores presumed to cause skin autofluorescence are uniformly distributed throughout the skin. The chlorophyll fluorescence component image shows strong fluorescence localized to the gut, as expected. (b) Technique 2 results in weak unmixed chlorophyll fluorescence and strong skin autofluorescence concentrations indicating that this technique results in a poor spectral definition of the two component spectra. The relative strengths of the spectral intensities are likely due to the uncommonly sharp shape of the chlorophyll fluorescence spectrum and its close overlap with the peak of the skin autofluorescence spectrum. (c) Robust spectral definition of skin autofluorescence results in the expected ratio between the spectral component concentrations and, additionally, results in the anticipated physiological spatial distributions of the two spectral components. Images have been scaled on the same absolute concentration scale to enable comparison of relative spatial distributions.

baseline days. A mixed fluorescence spectrum was sampled from the gut region of animals in the baseline phase [yellow line, Fig. 2(b)]. The skin autofluorescence spectrum was subtracted from the mixed spectrum resulting in a pure chlorophyll fluorescence spectrum [Fig. 3(b)]. However, because the tail of the animal has a slightly different skin autofluorescence spectrum than the skin itself and chlorophyll fluorescence was shown to be present in small concentrations on the tail during baseline, this method is likely to be suboptimal.

The robust spectral definition technique utilized in this study sampled skin autofluorescence spectra from the depilated upper abdominal region of animals that had been on a chlorophyll-free diet for 11 days [blue line, Fig. 2(c1)] and mixed fluorescence spectra from the gut region of animals in

the baseline phase [yellow line, Fig. 2(c2)]. The skin autofluorescence spectrum from the depilated upper abdominal area was subtracted from the mixed spectrum resulting in a pure chlorophyll fluorescence spectrum that proved itself to be superior to the comparable spectra resulting from techniques 1 and 2 [Fig. 3(c)].

2.3 Imaging Methods

All of the data presented herein was acquired using the yellow Maestro filter set, which employs a 575 to 605 nm excitation filter and a 645 nm longpass emission filter, with spectral imaging data collected in 10 nm steps between 630 and 850 nm using a liquid crystal tunable filter (LCTF) system.

The LCTF functions as a tunable bandpass filter by employing electronically controlled liquid crystal retardation waveplates arranged within a Lyot filter.²⁵ Multispectral image cubes were generated by capturing images as the transmission band of the LCTF was stepped discretely through a predefined emission spectral range. Exposure times of 1 s per step, 1 × 1 camera binning, lens *f*/# of 2.8, stage height 1, illumination arm height 1, and a full ROI were used for all image acquisitions.

Spectral unmixing, or the mathematical separation of linearly summed fluorescence emissions into distinct component images,^{20,26} was performed using the system software's unmixing function, resulting in spectral component maps of component concentration at each time point.^{21,27,28} Determination of unknown spectra from different fluorescent sources was performed by taking advantage of the fact that mixed spectra combine linearly and are imaged as such. In an experiment employing *N* defined component spectra, *a priori* knowledge of the spectral shapes of *N*−1 of the components enables calculation of the unknown spectra from the detected spectral curves. The measured spectral intensity at an arbitrary pixel in an experiment employing two component spectra, one of which is known previously, is given by

$$I(\lambda) = K(\lambda) + U(\lambda), \quad (1)$$

where $I(\lambda)$ is the measured intensity, $K(\lambda)$ is the known spectrum, and $U(\lambda)$ is the unknown spectrum.^{21,29} Subtraction of $K(\lambda)$ from $I(\lambda)$ provides the shape of $U(\lambda)$. This is the method most often used to determine the *in vivo* spectra of common exogenous fluorophores: autofluorescence is measured from an unlabeled control animal, and a mixed fluorescence spectrum consisting of autofluorescence and fluorescence from the fluorophore is measured from a labeled animal. The exogenous fluorophore's *in vivo* spectrum is then calculated via similar spectral subtraction to Eq. (1). Once the component spectra shapes are identified, spectral unmixing proceeds on a pixel-by-pixel basis

$$I(x, y, \lambda) = C_1 K(\lambda) + C_2 U(\lambda), \quad (2)$$

where $I(x, y, \lambda)$ is the measured intensity at wavelength λ at pixel x, y ; C_i is a linear weighting coefficient; and $K(\lambda)$ and $U(\lambda)$ are the previously determined spectra. An inverse least-squares fit is performed to determine the weighting coefficients, C_i . Common unmixing algorithms force the C_i 's to sum to unity due to physiological considerations and to enable comparison between spectral component images.^{21,27} Once the C_i 's are determined, quantitative determination of each fluorophore at every pixel of an acquired multispectral image is then possible.

Longitudinal tracking of spectral component concentration was accomplished using an elliptical measurement ROI. One ROI was used for each spectral component and its shape and size was chosen to best accommodate the average spatial distributions of the spectral component concentrations during the baseline phase. Chlorophyll fluorescence measurement ROIs were placed over the gut where the highest chlorophyll fluorescence concentration was detected. Skin autofluorescence measurement ROIs were placed over the depilated region

above the gut away from the high chlorophyll concentration present there (spectral component images, Figs. 4–6).

2.4 Data Analysis Methods

Total spectral component concentration within a ROI across individual strains was averaged at each time point. The baseline value for each spectral component was taken as the mean of all baseline measurements. All subsequent time points were normalized to the baseline value, with the standard error of the mean (SEM) taken as the error. Normalized time courses tracking concentration changes in each spectral component were generated from these values and are shown in Figs. 4–6 with the SEM as the error bars.

3 Results

The first result required when performing an *in vivo* multispectral imaging study, longitudinal or otherwise, is the development of a library of component spectra produced by the chosen spectral definition technique. Figure 3 shows skin autofluorescence and chlorophyll fluorescence spectra resulting from the three spectral definition techniques investigated herein. All spectra have been normalized to their respective maximum values to better illustrate wavelength-dependent behavior on the same plot. Additionally, Fig. 3 shows examples of unmixed spectral component images from a baseline day.

The first comparison spectral definition technique, with skin autofluorescence sampled from the tail and chlorophyll fluorescence sampled from the gut on a baseline day [Fig. 2(a)], results in component spectra exhibiting moderately close wavelength-dependent behavior, with both spectra peaking within an approximately 10 nm band and poor spectral separation about the common peak [Fig. 3(a)]. This suboptimal result is due to the sampling method employed by technique 1. By sampling on a baseline day, both of the component spectra were present in varying concentrations across the surface of the animal. Skin autofluorescence was more intense than chlorophyll fluorescence in the tail while the opposite was true over the gut. The two sampled spectra derived from these regions should show approximately the same behavior because they are different linear mixings of the two defined component spectra. Technique 1 produces unmixed skin autofluorescence component images with large regions of zero concentration, spatially localized within regions of high chlorophyll fluorescence concentration in the gut. Chlorophyll fluorescence is found strongly localized to the gut with some of the underlying digestive structure visible.

The second comparison spectral definition technique sampled skin autofluorescence from a depilated chest region, mixed fluorescence from the gut on a baseline day, and calculated chlorophyll fluorescence from the sampled spectra [Fig. 2(b)]. Technique 2 results in a highly unusual chlorophyll fluorescence spectrum: a peak confined to an approximately 50 nm band, with a slightly broader skin autofluorescence spectrum than the one produced by the first spectral definition technique [Fig. 3(b)]. The skin autofluorescence component image in Fig. 3(b) shows localized regions of high concentration around the gut with most of the same underlying digestive structure seen in Fig. 3(a)'s chlorophyll component image readily visible. The chlorophyll component image shows strong localization to the gut but not the expected con-

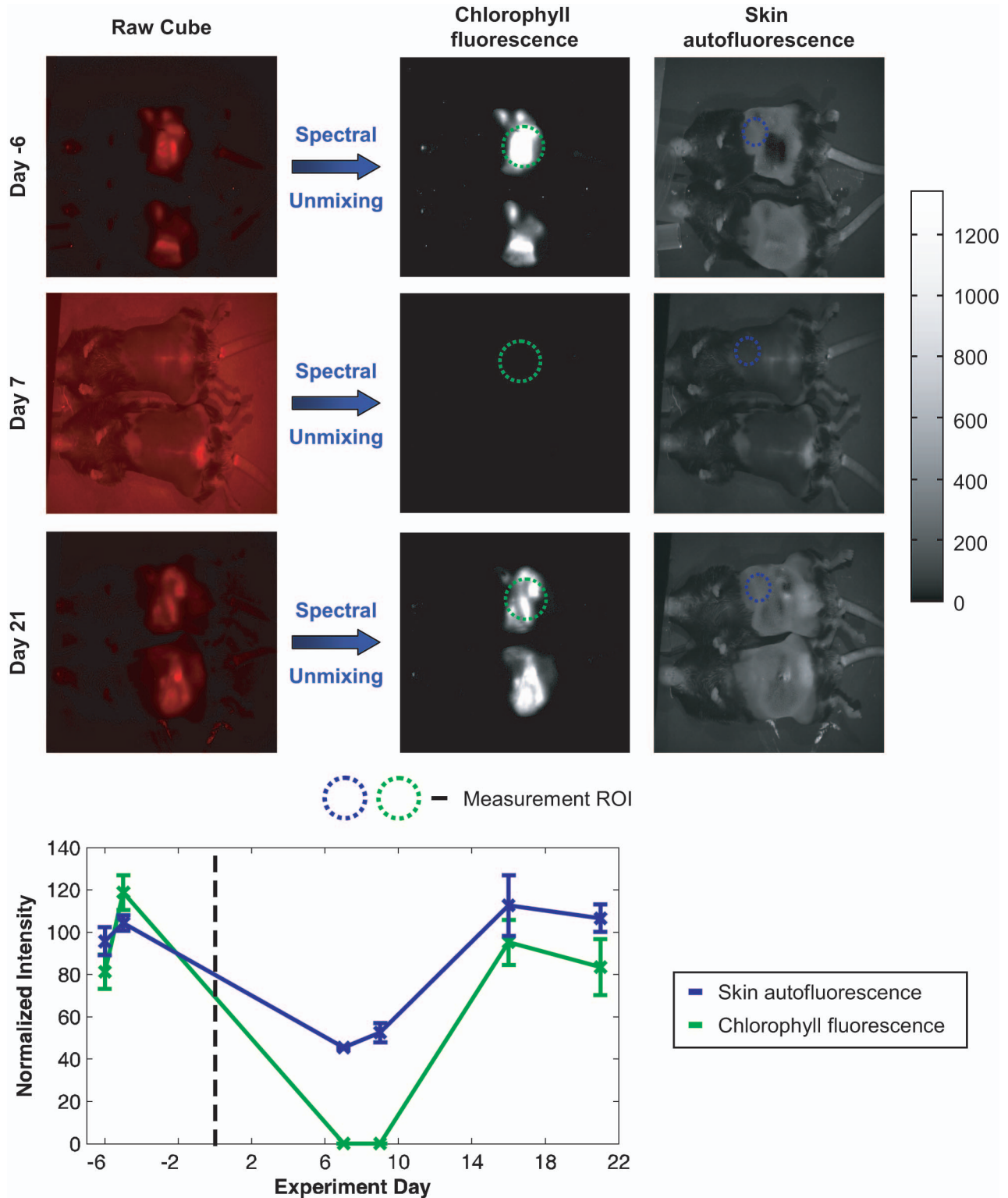


Fig. 4 Technique 1 results. Chlorophyll fluorescence and skin autofluorescence sampled on a baseline day without performing a pure spectral calculation to determine pure component spectra results in implausible spectral component behavior. On baseline and return days, the skin autofluorescence component images display large regions of near-zero skin autofluorescence concentration, spatially localized within regions of high chlorophyll component concentration in the underlying digestive tissue. Skin autofluorescence concentration is expected to be spatially uniform across the skin because it is caused by fluorophores endogenous to mouse skin, not chlorophyll and its fluorescent derivatives. Chlorophyll fluorescence component images are seen to follow the expected time course, but only around the gut region; usually small amounts of chlorophyll fluorescence are detectable on the snout and paws due to adherent chlorophyll fluorophores remaining in the animal cages during the no-glow phase in the form of small food particles, urine, and feces. Images have been scaled on the same absolute concentration scale to enable comparison of relative spatial distributions.

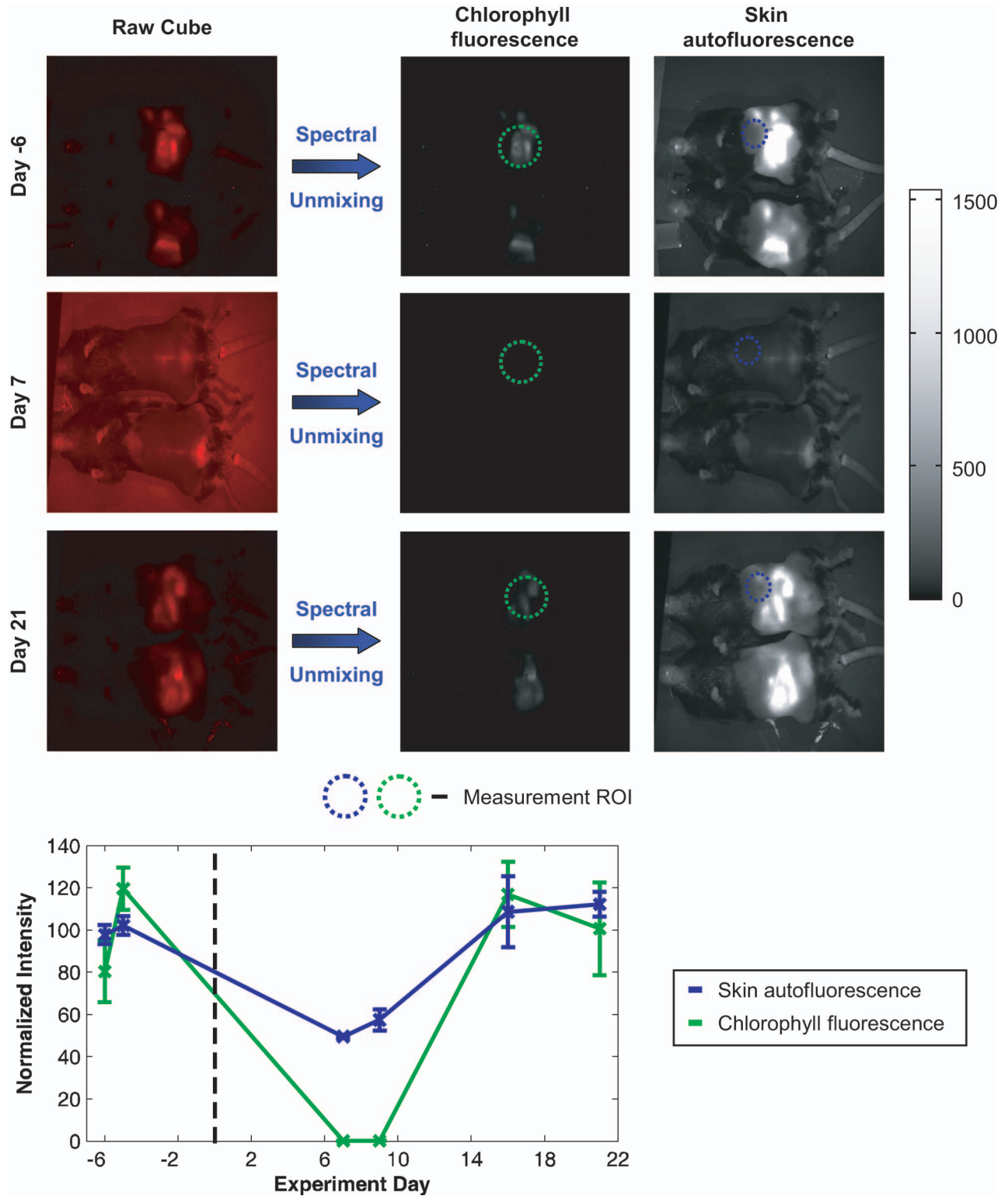


Fig. 5 Technique 2 results. Chlorophyll fluorescence calculated from mixed fluorescence and skin autofluorescence sampled on a baseline day results in implausible spectral component behavior. Both spectral components show dramatic concentration changes over the course of the study with the average skin autofluorescence signal more intense than chlorophyll fluorescence in an approximately 10:1 ratio throughout. In addition, skin autofluorescence concentration is not expected to change dramatically because it is caused by fluorophores endogenous to mouse skin, not chlorophyll and its fluorescent derivatives. Images have been scaled on the same absolute concentration scale to enable comparison of relative spatial distributions.

centration relative to the skin autofluorescence component. Technique 2 results in an approximately 10:1 skin autofluorescence to chlorophyll fluorescence ratio over the gut; normally this ratio is inverted due to chlorophyll's stronger fluorescence signal.¹⁴

The standard, robust spectral definition technique, with skin autofluorescence sampled from a depilated chest region on the last day of the no-glow phase, mixed fluorescence sampled from the gut on a baseline day, and chlorophyll fluorescence calculated from the sampled spectra [Fig. 2(c)] results in the most pronounced spectral separation between the two component spectra achieved in this study [Fig. 3(c)]. It can be seen from the spectra in Fig. 3(c) that the skin autofluorescence spectrum is much broader about the common peak, indicating it is composed of a broad range of fluorophores such as those found in murine skin. Unmixing using the robust technique shows skin autofluorescence distributed throughout the depilated regions of the skin with a slight increase in intensity about the gut region. Chlorophyll fluorescence is seen localized to the gut region with a high degree of spatial separation between the gut and the surrounding depilated skin. During the no-glow phase of the study, weak chlorophyll fluorescence that is normally masked by the higher signal emitted from the gut is visible on the snout and paws, in the bladder, and on the base of the tail, regions that do not show chlorophyll fluorescence in the other spectral definition techniques (component images, Figs. 4–6).

Once the component spectra are defined, the next step is to unmix each of the raw multispectral image cubes using the same spectral library and then quantify the changes in spectral component concentration over time. The time-dependent behavior of the skin autofluorescence concentrations resulting from the three spectral definition techniques reveals striking differences (blue line, time course plots, Figs. 4–6). Skin autofluorescence is presumed to remain constant within normal experimental variation throughout the study. Comparison techniques 1 and 2 produce time courses with approximately 50% drops in skin autofluorescence concentration during the no-glow phase of the study. These large declines in signal are likely due to the fact that the skin autofluorescence spectra utilized for each technique are actually mixtures of skin autofluorescence and chlorophyll fluorescence, that is, they are “mixed” spectra composed of skin autofluorescence plus some contribution from chlorophyll fluorescence, not the pure spectra required for effective multispectral imaging studies. The robust spectral definition technique resulted in the most stable of the three skin autofluorescence time courses (Fig. 6). However, it does show a slight drop temporally coupled with the removal of chlorophyll from the diet, again indicating impure spectral definition of the component spectra.

Chlorophyll fluorescence is presumed to remain stable within normal food consumption variability on baseline days and decrease to a stable, near-zero concentration while in the no-glow phase. The rate of concentration decay is proportional to the rate of food consumption and passage of food through the digestive system. In the return phase, the concentration should return to approximately the baseline level. Across all three techniques, chlorophyll fluorescence concentration is seen to decrease to near zero while in the no-glow phase, as expected. However, the techniques differ in the consistency of their baseline values and how closely they ap-

proach zero concentration while in the no-glow phase (green line, time course plots, Figs. 4–6). Comparison techniques 1 and 2 produce largely varying baseline values, but the return phase does not perform as expected when utilizing the robust technique. Additionally, comparison techniques 1 and 2 show concentrations that approach within 0.04% of zero at their closest approach while in the no-glow phase. The robust technique approaches within 0.8% of zero in the same phase.

4 Discussion

The technical challenge presented to robust spectral definition by the autofluorescence-reduction study included determining the best spatiotemporal location from which to sample each spectral component. If one assumes that chlorophyll fluorescence only localizes to the digestive system, it should be simple to spectrally define skin autofluorescence. This assumption requires that the fluorophores underlying chlorophyll fluorescence are broken down by the digestive process and no longer emit the same fluorescence spectrum when circulated throughout the body. Under this assumption, skin autofluorescence should be sampled on a baseline day and measured in a depilated region of the animal away from the gut (i.e. the chest region or the large leg muscles). A chlorophyll fluorescence spectrum could then be calculated from the mixed fluorescence sampled from the gut. However, the autofluorescence-reduction study confirmed our initial assumption that chlorophyll fluorescence does not spatially localize to the digestive system, but causes a whole-body effect due to the circulation of digested chlorophyll fluorophores.²³ For this reason, it is necessary for robust spectral definition to sample skin autofluorescence spectra from the final time point of the No-glow-phase because this is when the chlorophyll fluorescence concentration in the skin is at its minimum.

Spectral definition technique 1, however, did not obtain component spectra using a pure spectral calculation with sampled spectra. The component spectra resulting from technique 1 were different linear mixings of the two defined component spectra. By sampling chlorophyll fluorescence over the gut, its defined spectrum was more strongly represented in the sampled spectrum than the weaker skin autofluorescence spectrum. The inverse was true for skin autofluorescence measured away from the higher concentration of chlorophyll fluorescence in the gut. Technique 1's skin autofluorescence component images show large regions of zero concentration spatially localized within regions of high chlorophyll concentrations in the gut [Figs. 3(a) and 4]. Because the chlorophyll fluorescence spectrum was measured directly from the gut, the spectral unmixing algorithm assigned nearly 100% of the mixed fluorescence signal present there to the chlorophyll component. In the no-glow phase of the study, no chlorophyll fluorescence signal is detected in any region of the animal, contradicting the observation that chlorophyll containing compounds are visible on the surface of the animal mostly due to circulation and adherent chlorophyll fluorophores remaining in the animal cages. Interestingly, the regions of the animal away from the gut in the skin autofluorescence component images approximately show the spatiotemporal behavior expected of them. In the no-glow phase of the study, there is a slight degree of skin autofluorescence spatial localization to the gut and bladder with an approximately uniform concen-

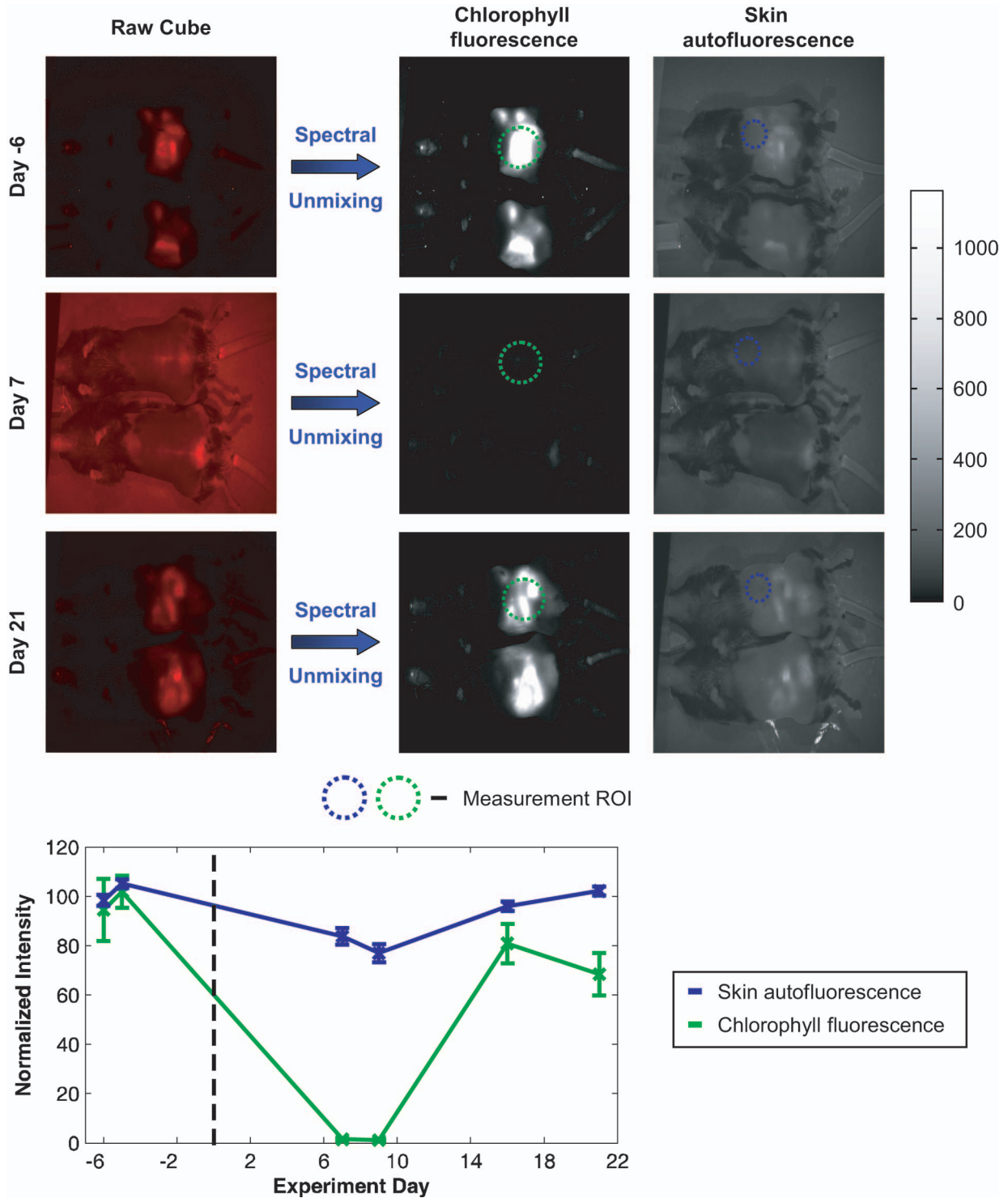


Fig. 6 Technique 3 results. Mixed fluorescence sampled from the gut on a baseline day, skin autofluorescence sampled from the upper abdominal region on the last time point of the chlorophyll-free diet, and chlorophyll fluorescence calculated from the sampled spectra produces the most robust spectral definition and physiologically plausible results obtained by the three investigated spectral definition techniques. Both spectral component images exhibit most of the expected spatiotemporal behavior of them, with skin autofluorescence displaying a slight increase in concentration in the gut during the baseline and return phases of the study. Although the skin autofluorescence time course does display a slight dip temporally coupled to the removal of chlorophyll from the diet, it displays the least dramatic drop of the three spectral definition techniques. This is likely due to imperfect spectral separation of the two defined spectra. The chlorophyll fluorescence time course and spectral component images follow the predicted temporal behavior with a slight underperformance seen in the time course during the return phase of the study. Additionally, relatively weak concentrations of chlorophyll fluorescence localized to the snout and paws, in the bladder, and on the base of the tail are clearly visible in the day 7 component image when not masked by the high concentrations at the beginning and end of the study. Spectral definition techniques 1 and 2 fail to show chlorophyll fluorescence in these locations at any point in the study. Images have been scaled on the same absolute concentration scale to enable comparison of relative spatial distributions.

tration elsewhere that is smaller in value than the other two phases of the study. This result supports the conclusion that the sampled spectra defined by technique 1 contained portions of both defined spectra and produced physiologically implausible results.

Spectral definition technique 2 utilized a tail spectrum for skin autofluorescence and a calculated chlorophyll fluorescence spectrum [Fig. 2(b)]. Because the autofluorescent components of the tail are different than the rest of the skin, it is not clear that this technique will be optimal. That these spectra form a suboptimal spectral library is further supported by the tight spatial localization of skin autofluorescence to the gut and the inverted ratio of skin autofluorescence to chlorophyll fluorescence concentration in the gut as seen in Fig. 2(b), in addition to the large trough in the skin autofluorescence time course shown in Fig. 5. Additionally, by sampling skin

autofluorescence from the tail, spectral definition techniques 1 and 2 have introduced two additional routes for poor spectral definition to occur: residual chlorophyll fluorescence on the tail from adherent fluorophores and the different autofluorescent component composition of the tail.

Following the confirmation that chlorophyll fluorescence is a whole-body effect that needs to be reduced below detectable levels for effective spectral definition of skin autofluorescence, one is driven to the robust spectral definition technique and sampling skin autofluorescence from regions of an animal's body away from the gut on the last day of the no-glow phase of the study (spectral definition technique 3). If chlorophyll fluorophores were present at this time point, they would be in their lowest concentration, enabling the most robust definition of skin autofluorescence possible within the confines of the autofluorescence-reduction study design. After robust definition of skin autofluorescence, chlorophyll fluorescence can be calculated from mixed fluorescence sampled on a baseline day and the no-glow skin autofluorescence spectrum. It is possible that the skin autofluorescence spectrum changes in shape and intensity as a result of removal of chlorophyll from the diet, thus negatively affecting the value of the unmixed skin autofluorescence concentration and subsequent component images. A future study employing better controls for chlorophyll fluorescence could assess these hypotheses.

Comparison of the time courses shown in Figs. 4–6 shows the expected result that robust spectral definition produces time courses most closely approximating the expected spectral component temporal behavior. Additionally, inspection of the results from the unmixed spectral component images shown in Fig. 6 reveals none of the implausible physiological characteristics associated with spectral definition techniques 1 and 2. However, the robust spectral definition technique's skin autofluorescence time course does drop in conjunction with removal of chlorophyll from the diet and its component images do show a greater concentration of skin autofluorescence about the gut with some of the underlying digestive structure visible in the baseline and return images. This spatial distribution is likely due to the poor spectral separation about the components' common peak due to imperfect spectral definition, possibly resulting from the autofluorescence-reduction study's lack of an adequate control for chlorophyll fluorescence [Fig. 3(c)].

Also of interest in Fig. 6 is that in its day 7 unmixed component image chlorophyll fluorescence is visible in small concentrations on the snout and paws, in the bladder, and on the base of the tail, regions where chlorophyll fluorescence is not visible in the unmixed component images of the other two spectral definition techniques (Figs. 4 and 5). Small fragments of standard chow should be found on the surface of the animal body in regions such as the snout and paws, in the bladder, and on the base of the tail. These fragments originated from adherent fluorescent food particles, urine, and feces that remained in the animal cages because our animal facility operates on a 14-day cycle, overlapping the no-glow phase of the study. The ability to detect these weak signals with the robust spectral definition technique, and not the comparison techniques, is further evidence of its robustness.

5 Conclusion

We have shown that the effective use of *in vivo* multispectral imaging techniques requires comprehensive physiological understanding of the defined component spectra. On their own, the algorithms employed by multispectral imaging techniques do not provide the ability to accurately define relevant and robust spectra. A certain amount of *a priori* knowledge of fluorophore spatial distribution *in vivo* is required for physiologically appropriate use of multispectral imaging techniques.

Acknowledgments

The authors would like to thank Gordon Turner for the many helpful discussions and Emil Fu and Michael Smith for continuous support.

References

1. J. A. DiMasi, R. W. Hansen, and H. G. Grabowski, "The price of innovation: New estimates of drug development costs," *J. Health Econ.* **22**(2), 151–185 (2003).
2. C. P. Adams and V. V. Brantner, "Estimating the cost of new drug development: Is it really 802 million dollars?," *Health Aff (Millwood)* **25**(2), 420–428 (2006).
3. J. Drews, "Drug discovery: A historical perspective," *Science* **287**(5460), 1960–1964 (2000).
4. C. Deboucq and P. N. Goodfellow, "DNA microarrays in drug discovery and development," *Nat. Genet.* **21**(1 Suppl), 48–50 (1999).
5. SMI, "The Society for Molecular Imaging, presented at the Fifth Annual Meeting of the Society for Molecular Imaging 2006, Waikoloa, Hawaii.
6. M. Rudin and R. Weissleder, "Molecular imaging in drug discovery and development," *Nat. Rev. Drug Discovery* **2**(2), 123–131 (2003).
7. X. Gao, Y. Cui, R. M. Levenson, L. W. Chung, and S. Nie, "*In vivo* cancer targeting and imaging with semiconductor quantum dots," *Nat. Biotechnol.* **22**(8), 969–976 (2004).
8. R. Weissleder and V. Ntziachristos, "Shedding light onto live molecular targets," *Nat. Med.* **9**(1), 123–128 (2003).
9. B. W. Rice, M. D. Cable, and M. B. Nelson, "*In vivo* imaging of light-emitting probes," *J. Biomed. Opt.* **6**(4), 432–440 (2001).
10. P. R. Contag, I. N. Olomu, D. K. Stevenson, and C. H. Contag, "Bioluminescent indicators in living mammals," *Nat. Med.* **4**(2), 245–247 (1998).
11. D. Huang et al., "Optical coherence tomography," *Science* **254**(5035), 1178–1181 (1991).
12. J. R. Mansfield and R. M. Levenson, "Distinguished photons: The Maestro™ *in-vivo* Fluorescence Imaging System," *BioTechniques Protocol Guide 2006* (2007), pp. 49–62.
13. J. R. Mansfield, C. C. Hoyt, P. J. Miller, and R. M. Levenson, "Distinguished photons: Increased contrast with multispectral *in-vivo* fluorescence imaging," *BioTechniques* **39** (Suppl.), S25–S29 (2005).

14. T. Troy, D. Jekic-McMullen, L. Sambucetti, and B. Rice, "Quantitative comparison of the sensitivity of detection of fluorescent and bioluminescent reporters in animal models," *Mol. Imaging* **3**(1), 9–23 (2004).
15. P. J. Miller and C. C. Hoyt, "Multispectral imaging with a liquid crystal tunable filter," *Proc. SPIE* **2345**, 354–365 (1995).
16. G. Bearman and R. Levenson, *Biological Imaging Spectroscopy*, CRC Press, Boca Raton, FL (2003).
17. G. Zavattini, S. Vecchi, G. Mitchell, U. Weisser, R. M. Leahy, B. J. Pichler, D. J. Smith, and S. R. Cherry, "A hyperspectral fluorescence system for 3D *in vivo* optical imaging," *Phys. Med. Biol.* **51**(8), 2029–2043 (2006).
18. S. Tominaga, "Spectral imaging by a multichannel camera," *J. Electron. Imaging* **8**(4), 332–341 (1999).
19. J. M. Tam, R. Upadhyay, M. J. Pittet, R. Weissleder, and U. Mahmood, "Improved *in vivo* whole animal detection limits of GFP-expressing tumor lines by spectral fluorescence imaging," *Mol. Imaging* **5**(3), Abstract 231, 244 (2006).
20. T. Zimmermann, J. Rietdorf, A. Girod, V. Georget, and R. Pepperkok, "Spectral imaging and linear un-mixing enables improved FRET efficiency with a novel GFP2-VFP FRET pair," *FEBS Lett.* **531**(2), 245–249 (2002).
21. R. Lansford, G. Bearman, and S. E. Fraser, "Resolution of multiple green fluorescent protein color variants and dyes using two-photon microscopy and imaging spectroscopy," *J. Biomed. Opt.* **6**(3), 311–318 (2001).
22. D. L. Farkas, C. Du, G. W. Fisher, C. Lau, W. Niu, E. S. Wachman, and R. M. Levenson, "Non-invasive image acquisition and advanced processing in optical bioimaging," *Comput. Med. Imaging Graph.* **22**(2), 89–102 (1998).
23. S. A. MacLaurin, M. Bouchard, P. Dwyer, R. Levenson, J. Mansfield, and T. Krucker, "Reduction of skin and food autofluorescence in different mouse strains through diet changes," *Mol. Imaging* **5**(3), Abstract 523, 252 (2006).
24. G. Weagle, P. E. Paterson, J. Kennedy, and R. Pottier, "The nature of the chromophore responsible for naturally occurring fluorescence in mouse skin," *J. Photochem. Photobiol., B* **2**(3), 313–320 (1988).
25. H. R. Morris, C. C. Hoyt, and P. J. Treado, "Imaging spectrometers for fluorescence and raman microscopy: Acousto-optic and liquid crystal tunable filters," *Appl. Spectrosc.* **48**(7), 857–866 (1994).
26. M. E. Winter, "N-FINDR: An algorithm for fast autonomous spectral end-member determination in hyperspectral data," *Proc. SPIE* **3753**, 266–275 (1999).
27. J. R. Mansfield, K. W. Gossage, C. C. Hoyt, and R. M. Levenson, "Autofluorescence removal, multiplexing, and automated analysis methods for *in-vivo* fluorescence imaging," *J. Biomed. Opt.* **10**(4), 041207 (2005).
28. M. E. Dickinson, G. Bearman, S. Tille, R. Lansford, and S. E. Fraser, "Multispectral imaging and linear unmixing add a whole new dimension to laser scanning fluorescence microscopy," *BioTechniques* **31**(6), 1272, 1274–1276, 1278, (2001).
29. T. Zimmermann, J. Rietdorf, and R. Pepperkok, "Spectral imaging and its applications in live cell microscopy," *FEBS Lett.* **546**(1), 87–92 (2003).